The Thesis Committee for Gabriella Marie Gregson Coloyan
Certifies that this is the approved version of the following thesis:

Basal Plane Thermal Conductivity of Thin Germanane Layers

APPROVED BY
SUPERVISING COMMITTEE:

Supervisor:

Li Shi

Yaguo Wang

Basal Plane Thermal Conductivity of Thin Germanane Layers

by

Gabriella Marie Gregson Coloyan, B.S.M.E.

Thesis

Presented to the Faculty of the Graduate School of
The University of Texas at Austin
in Partial Fulfillment
of the Requirements
for the Degree of

Master of Science in Engineering

The University of Texas at Austin
May 2014

Acknowledgements

I would like to acknowledge our collaborators in the Josh Goldberger group at the Ohio State University for providing me with the Germanane samples, and Michael Pettes and Annie Weathers for fabricating the suspended microheaters. I would also like to thank Ms. Weathers for her help in teaching me the sample assembly process. Finally, I would like to thank my advisor, Dr. Li Shi, for all of his support and encouragement.

Abstract

Basal Plane Thermal Conductivity of Thin Germanane Layers

Gabriella M. G. Coloyan, M.S.E.
The University of Texas at Austin, 2014

Supervisor: Li Shi

The thermal conductivity of thin Germanane (GeH) layers was measured using suspended micro-devices with integrated heaters and thermometers. The thermal contact resistance of the GeH samples suspended on the measurement devices was determined from the measured thermal resistance values of samples with different suspended lengths. The room-temperature thermal conductivity of the GeH samples was observed to be 0.6-1.0 $Wm^{-1}K^{-1}$. This low thermal conductivity is attributed to phonon scattering by defects and grain boundaries in the layered materials, including scattering caused by gangling bonds associated with missing Hydrogen atoms between adjacent layers.

Table of Contents

List of Tables

List of Figures

Chapter 1

Introduction

In 2013, the United States consumed 97.4 quadrillion BTUs (Quads) of energy. This came from both natural resources, such as petroleum, coal, and natural gas; and renewable resources, such as solar, nuclear, hydro, and wind power. However, only 39% of this energy was actually used, and the rest was wasted, largely due to waste heat [1]. This waste can be manifested in a variety of sources, such as cars, laptops, personal computers, and other electronic devices. As natural resources run out, researchers have begun to develop novel solutions for energy generation.

Thermoelectric devices offer a potential solution to this energy problem. These devices use the Seebeck effect to convert a temperature gradient to an electrical potential. They are rapidly becoming more popular, as researchers seek next-generation devices for thermal management and energy conversion. As a significant portion of US energy is lost due to waste heat, thermoelectrics devices have received increasing interest for waste heat recovery.

1.1 Thermoelectricity in Nanoscale Systems

In order to determine if a material would be a good candidate for use in a thermoelectric device, the thermoelectric figure of merit ZT, must be calculated:

$$ZT = \frac{S^2 \sigma T}{\kappa} \tag{1.1}$$

where S is the Seebeck coefficient, σ is the electrical conductivity, T is the absolute temperature, and κ is the thermal conductivity of the material. Maximizing the thermoelectric figure of merit is challenging, as the three transport properties are related to each other. Typical *ZT* values are usually around unity, though there have been recent reports of *ZT* values as high as 2.6 [2].

1.2 Motivation of This Work

Carbon, Silicon, Germanium, and Tin belong to Group-IV elements. Among them, cubic phase Si_xGe_{1-x} with sp^3 covalent bonding has been investigated for use in thermoelectric devices. Meanwhile, the thermal properties of hexagonal layered graphite and graphene with sp^2 bonding in the basal plane have been extensively researched [3-6]. Work has also begun on characterization of the size effects of the thermal conductivity of silicon-germanium alloy thin films [7], as well as the properties of silicene [8], which is surface functionalized atomic layers of silicon. Recently, thin Germanane, which are stacks of hydrogen-terminated germanium (GeH) atomic layers, have been synthesized and predicted to possess useful electronic properties [9]. The thermal and thermoelectric properties of this novel material can influence its use in electronic and thermoelectric devices, and have remained largely unknown.

This objective of this work is to investigate the thermal conductivity of thin GeH layers. Thermal conductivity characterization is the first step to experimentally determining Germanane's thermoelectric figure of merit, and will help evaluate the potential of GeH for use in electronic and thermoelectric devices.

Chapter 2

Thermal Transport Measurements for Thin Films

Thermal property measurements in micro- and nanoscale materials are considerably more difficult than those for bulk materials. Microscale structures are difficult to manipulate, and require microscale thermometers. Issues such as heat loss due to radiation and contact resistance also need to be considered. A number of techniques have been developed to characterize the thermal properties of such materials, including Raman thermometry, time-domain thermoreflectance, the 3ω technique, and the use of suspended micro-devices. A review of these methods is presented in this chapter, as well as selection criteria for the measurement technique used to characterize the in-plane thermal conductivity of thin-film Germanane.

2.1 Raman Thermometry

Raman thermometry has been used to investigate the thermal conductivities of pristine graphene [10], as well as $TaSe_2$ and MoS_2 thin films [11, 12]. In this method, a laser is focused on a sample suspended across a circular hole, heating the surface. The heat is absorbed by the sample, yielding a temperature difference across it. The thermal conductivity is given by solving

$$\boldsymbol{\kappa}\frac{1}{r}\frac{d}{dr}\left[r\frac{dT_1(r)}{dr}\right]+q(r)=0 \qquad \text{for } r<R \qquad (2.1)$$

where $\boldsymbol{\kappa}$ is the thermal conductivity of the sample, $T_1(r)$ is the temperature distribution inside the hole, r is the radial position from the center of the hole, R is the hole radius, and $q(r)$ is the volumetric Gaussian heating caused by the laser.

In order to find $T_1(r)$, and therefore be able to calculate the thermal conductivity, Raman scattering spectroscopy is used. For a given material, the Raman peaks are measured. An example of Raman spectroscopy data for GeH on a silicon dioxide substrate is given in Figure 2.1 below. The peak position depends on the optical phonon energy, and can shift as the temperature of the sample changes because of the temperature dependence of the phonon dispersion. In such measurements, the micro-Raman laser beam is essentially both a heat source and a temperature probe. However, the Raman peak position is also influenced by doping and strains, which can be different between the calibration of the temperature dependence of the Raman peak position with uniform heating and the thermal conductivity measurement with localized laser heating.

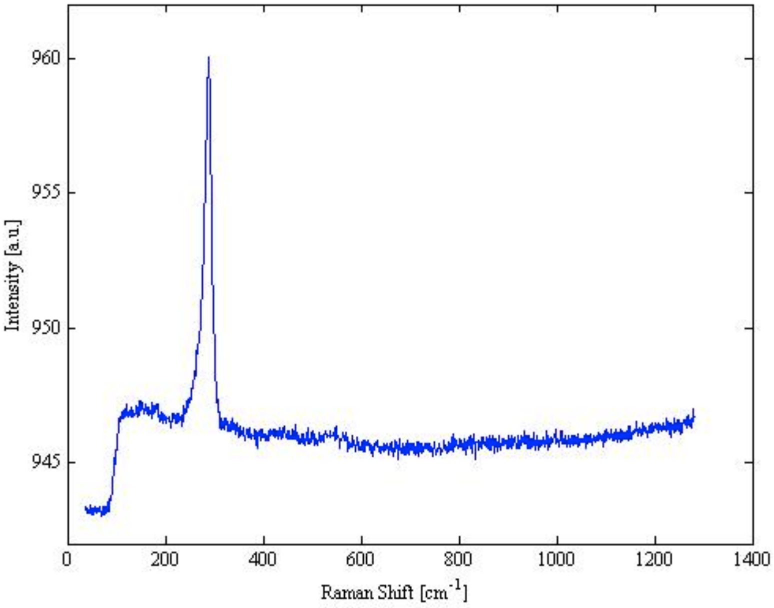

Figure 2.1: Raman spectroscopy data for supported GeH

While Raman thermometry is an available technique for characterizing the thermal conductivity of many thin-film materials, it is not well suited for measurements of suspended Germanane. Germanane is very temperature-sensitive, and is not able to survive the heating caused by the laser, even when the laser power is as low as possible. Suspending the samples makes it even more difficult for the heat from the laser to dissipate, since the sample is thermally isolated. It was found that collecting Raman data for even a short period of time burned holes in the samples, so that the samples would not be able to survive long Raman measurements needed for thermal measurements.

2.2 Time-Domain Thermoreflectance

Another common method used to measure the thermal conductivity of thin films is time-domain thermoreflectance (TDTR.) This method has been around for almost 30 years [13], and has recently been used to measure a wide range of materials, including $SrTiO_3$, silicon thin films, and nanocrystalline copper-carbon nanotube composites [14–16]. The basic principle behind the TDTR measurement technique is that the reflectance of a material changes as its temperature changes. To begin, the sample being studied is coated with a reflective metal, whose properties are already known. A laser beam is divided into two beams using a beam splitter, to be used as both the heating pump beam and the temperature probe beam. Using mirrors, both the pump and the probe beams are targeted at the same spot on the sample, and reflected back into photodetectors connected to lock-in amplifiers, which measure the signal from the lasers, and give values for reflectivity change as a function of temperature [17]. The thermal conductivity can be calculated by solving the one-dimensional conduction heat transfer equation

$$C\frac{\partial T(z,T)}{dt} = \kappa\frac{\partial^2 T(z,t)}{\partial z^2} + I(1-R)\alpha e^{-\alpha z} e^{(-t/\tau)^2} \qquad (2.2)$$

where $T(z,t)$ is the temperature profile of the sample, z is the distance perpendicular the sample surface, t is time, C is volumetric specific heat, κ is thermal conductivity, R is reflectivity, I is laser intensity, α is aborption per unit length, and τ is the laser pulse width. The sample temperature profile is calculated using a Simplex fitting routine that minimizes the mean-square difference between the normalized solutions to Eq. 2.2 and the profile from the TDTR experiments.

Germanane is an anisotropic material, due to its layered structure, as discussed in Chapter 3. The TDTR technique would only allow for measurement of its cross-plane thermal conductivity, whereas this project sought to characterize its in-plane thermal conductivity. Furthermore, in order to calculate thermal conductivity, the value of volumetric heat capacity must be known. Germanane is a new material, and this property has not yet been characterized, so a complete analysis would not have been able to be conducted.

2.3 3-Omega Method

The 3-omega, or 3ω, method developed by Cahill [18] is another popular experimental technique used to characterize the thermal conductivity of thin films. The 3ω experiments have been used to determine the thermal conductivity of polyaniline fibers and polycrystalline aluminum nitride thin films [19, 20]. In this measurement method, a metal line heater and electrode pads are deposited directly on top of the sample.

The line heater is then connected to a lock-in amplifier, and a sinusoidal current with frequency ω, $I(\omega)$, is applied. This current induces a heat flux oscillating at frequency 2ω, and a resultant voltage from Ohm's law, $V = IR$, at frequency 3ω can be measured. Similar to reflectivity in the TDTR method, in the 3ω method, the resistance of the line heater changes with respect to temperature. The thermal conductivity of the sample is obtained as:

$$\kappa = \frac{V^3 \ln f_2/f_1}{4\pi l R^2 (V_{3,1} - V_{3,2})} \frac{dR}{dT} \tag{2.3}$$

where κ is the sample thermal conductivity, V is the voltage across the line heater at frequency ω, l is the line heater length, $V_{3,1}$ is the in-phase 3ω voltage at frequency f_1, $V_{3,2}$ is the in-phase 3ω voltage at frequency f_2, and R is the average line heater resistance. More detailed analyses have been conducted by Wang and Sen [21] and Tong and Majumdar [22].

Though this method seemed a viable option for Germanane thermal conductivity measurements, it was ultimately decided that the suspended microheater technique was the best to use.

2.4 Suspended Microheater Technique

The technique chosen for Germanane thermal conductivity characterization is the suspended microheater technique developed by Shi *et al.* [23]. For fabrication of the micro-heater device, electron beam lithography (EBL) is used to pattern serpentine Pt resistance heaters and thermometers on a silicon nitride (SiN_x) coated Si wafer. Two platinum resistance thermometers (PRTs) on patterened SiN_x membranes make up each device. The Si underneath the SiN_x membranes is etched away using tetramethylammonium hydroxide, leaving the membranes each suspended by six thin SiN_x beams. The samples are placed on top of the two membranes, bridging the gap between them, as a thermal bridge. Suspending the membranes serves two purposes. Primarily, it thermally isolates the sample, so that heat cannot leak directly into the substrate. Secondarily, it allows for transmission electron microscopy (TEM) characterization of the sample after experiment completion. The rest of the device is comprised of bonding pads that allow for electrically connecting the device to the lock-in amplifiers used to make measurements.

The heat transfer in the system can be modeled as a simple conduction problem. The heat flows through the supporting beams and the sample, which can be modeled as resistors in series. G_s and G_b are the thermal conductances of the sample and supporting beams, respectively.

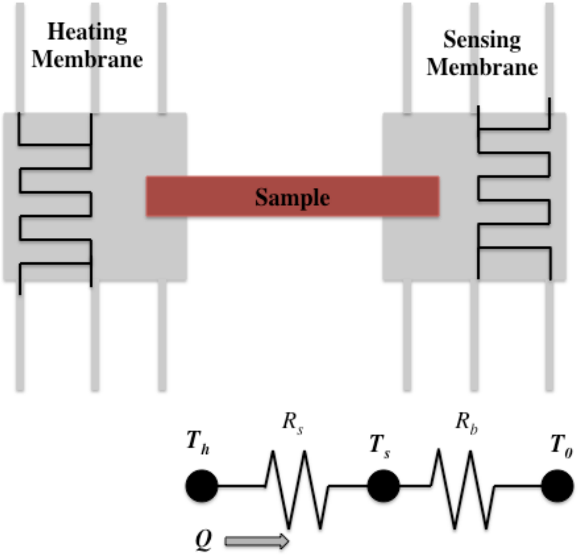

Figure 2.2: Schematic thermal resistance circuit of experimental setup, where $GR_b = \frac{1}{G_b}$ and $R_s = \frac{1}{RR_s}$ are the thermal resistances of the sample and the supported beams of one membrane

The heat flows through the suspended sample and the supporting beams of the sensing membrane, and can be obtained from the thermal resistance circuit as

$$Q = G_b(T_s - T_0) = G_s(T_h - T_s) \tag{2.4}$$

Each of the two Pt leads connected to the Pt serpentine dissipates Joule heat of $Q = I^2R$, where R is the electrical resistance of one Pt lead. Similarly, the Joule heat dissipated in the Pt serpentine heater is Q_h. The thermal resistances in the six supporting beams and in the sample can be obtained as:

$$R_b = \frac{\Delta T_h + \Delta T_s}{Q_h + Q_L} \tag{2.5}$$

$$R_s = R_b \frac{\Delta T_h - \Delta T_s}{\Delta T_s} \tag{2.6}$$

The temperature rises of the membranes, ΔT_h and ΔT_s, are obtained through measurements of the electrical resistance of the PRTs. A sweep of heating currents is supplied to the heating PRT, and the four-probe electrical resistance of the heating and sensing PRTs are measured using a lock-in amplifier, shown in Figure 1.3.

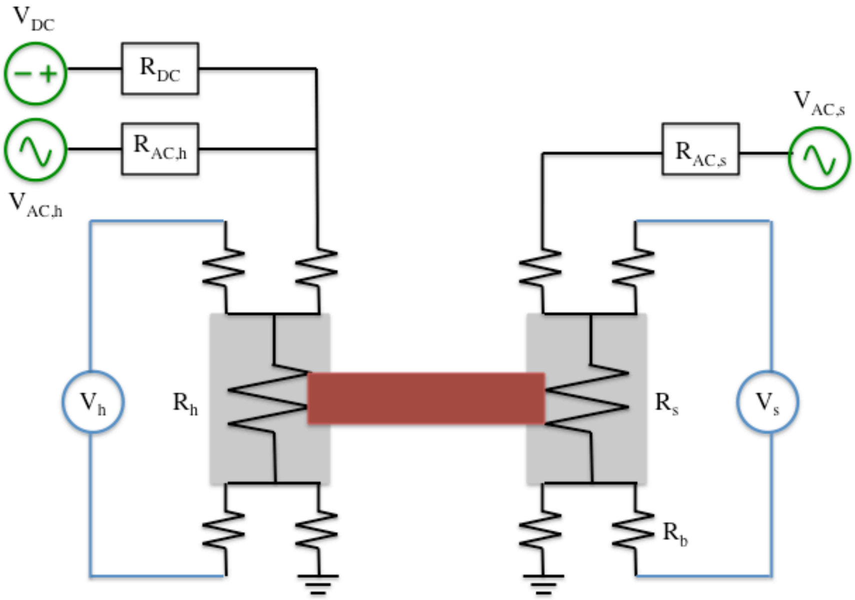

Figure 2.3: Schematic of experimental setup

$$\Delta T_h(I) = \frac{\Delta R_h(I)}{\frac{dR_h(I=0)}{dT}} \tag{2.7}$$

$$\Delta T_s(I) = \frac{\Delta R_s(I)}{\frac{dR_s(I=0)}{dT}} \tag{2.8}$$

where $\Delta R_h(I) = R_h(I) - R_h(I=0), \Delta R_s(I) = R_s(I) - R_s(I=0)$, and the temperature coefficients of resistance of the PRTs, $\frac{dR_h}{dT}$ and $\frac{dR_s}{dT}$, are found by measuring the resistances across a range of temperatures, plotting R_h vs. T and R_s vs. T, fitting a line to each of these curves, and taking their derivatives. It is worth noting that ΔR_h can be measured with high signal-to-noise ratio by coupling a small modulation current in the large heating current, and measuring the corresponding voltage modulation in the voltage drop across the Pt serpentine. For such measurements, Eq. 2.7 is only valid when the frequency of the small modulation current is sufficiently large compared to the thermal time constant of the system, so that the associated periodic heating yields negligible temperature modulation in the device. A frequency of about 2 kHz has been found to be sufficiently large for Eq. 2.7 for the suspended device [23].

Without accounting for the thermal contact resistance, the thermal conductivity of the sample can be determined after calculating the sample conductance:

$$\kappa = \frac{G_s L}{W t} \tag{2.12}$$

where G_s is the sample conductance, L is the sample length, W is the sample width, and t is the sample thickness.

This measurement technique can work well for the Germanane samples. The samples are not damaged by the measurement and are the right size for these devices. In addition, no assumptions need to be made about the intrinsic properties of the samples. However, it is important to account for the thermal contact resistance between the sample and the two membranes.

Chapter 3

Thermal Conductivity of Suspended Germanane

Germanane has recently been synthesized for the first time by Bianco *et al*. [9]. This process produces bulk flakes, which are then exfoliated and assembled onto suspended measurement devices. Metals were deposited through shadow masks onto the contact areas for one set of samples to improve contact between the samples and the devices, whereas this procedure was not used for the other set of samples. For both sets of samples, the contact thermal resistances were determined based on the measured thermal resistances of samples with different suspended lengths, so that the intrinsic thermal conductivity of suspended Germanane could be obtained. The thermal conductivity of the GeH samples was observed to be 0.6-1.0 $Wm^{-1}K^{-1}$ at room temperature. This low thermal conductivity is due to the short phonon mean free path. A detailed uncertainty analysis was also completed.

3.1 Material Synthesis and Background

The Germanane materials were synthesized by the Goldberger group at The Ohio State University, a process which involved a number of steps. First, β-$CaGe_2$ crystals were synthesized by placing stoichiometric ratios of calcium and germanium in a quartz tube, sealing the tube, annealing to 950-1050°C, and cooling for 2-10 days. The next step in GeH synthesis was topotactic deintercalation β-$CaGe_2$ in aqueous hydrochloric acid (HCl) at -40°C. This process took a minimum of eight days, and yielded high-purity $CaGe_2$. Finally, after the HCl step, the product was filtered and washed with methanol to yield GeH crystallites by removing leftover calcium chloride ($CaCl_2$.) These crystallites are in the form of silver-colored flakes, a few millimeters in diameter, and 100 microns thick. Mechanical exfoliation of these bulk flakes results in few-layer GeH that is 10 microns in diameter and 3 nm thick, and single-layer GeH 1 micron in diameter and 0.6 nm thick. Each of these layers can be considered sp^3-bonded hydrogen-terminated sheets of germanium, and each bulk flake consists of micron-thick stacks of these layers.

It was observed that GeH is a very temperature-sensitive material. Using Raman spectroscopy, it was determined that the structure becomes amorphous (a-GeH) at temperatures higher than 75°C. Additionally, thermogravimetric analysis showed a ~1.1% mass loss at 200-250°C, which is close to the expected mass loss from dehydrogenation, producing amorphous thin-film germanium (a-Ge.)

3.2 Sample Assembly Method

The samples were prepared by sonicating bulk GeH flakes in a vial containing acetone. Sonication decreased both the diameter of the flakes, as well as their thickness, to the order of tens of microns in the lateral dimension, and hundreds of nanometers in thickness. About 8 μL droplets of the solution were drop cast onto the suspended microheater devices, and samples were aligned manually on the device membranes using a sharp tungsten probe tip of a home-built micromanipulator.

In order to improve thermal contact between the sample and the membranes, a shadow masking- based metal deposition technique was used. This technique is essentially a micron-scale stenciling method. The shadow masks are fabricated using electron-beam lithography and reactive ion etching to open trenches in a SiN_x film grown on a silicon wafer. The silicon underneath the trench pattern was etched away using tetramethylammonium hydroxide, leaving a 500nm-thick suspended nitride membrane with four etched-through trenches. The shadow masks were aligned with the device, such that the trenches aligned with the sample and device electrodes using a Karl Suss MJB4 mask aligner. Finally, using an electron-beam metal evaporator, Palladium was deposited through the shadow mask and onto the sample. A sample after shadow masking and metal deposition is seen in Figure 3.1.

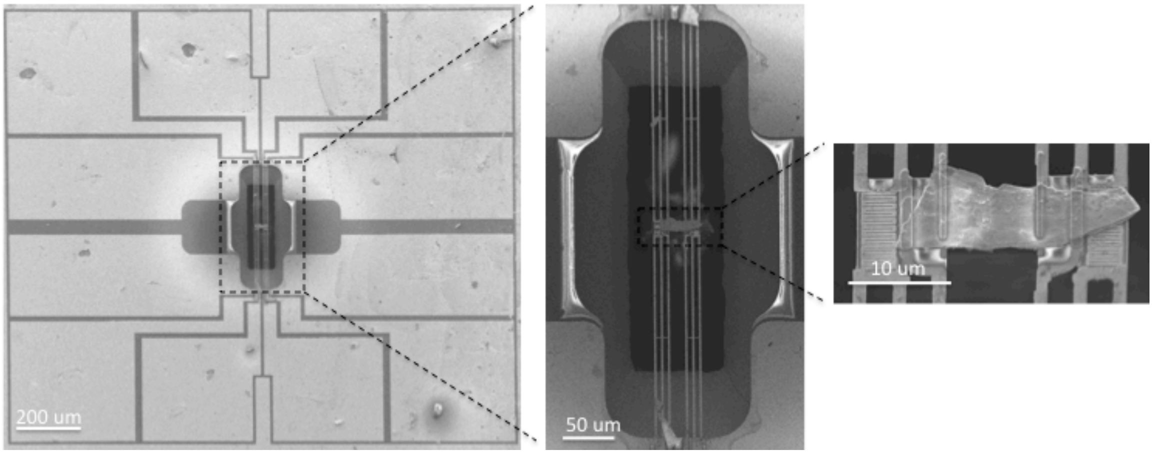

Figure 3.1: SEM image of a GeH sample after Pd deposition on four contacts

Germanane is known to undergo transition from crystalline to amorphous at temperatures above 75°C. While the temperature of the chamber stays well below the amorphization temperature during metal deposition, there were concerns that the sample may have seen higher temperatures, because of heating due to the deposited Pd atoms, as well as the condition that the sample is thermally isolated on the membranes, and the heat would not have been able to dissipate. Raman spectroscopy was unable to be used to determine if amorphization had occurred because the suspended samples were unable to survive the heat induced by the laser. To ensure that amorphization did not occur during metal deposition, two actions were taken.

First, transmission electron microscopy (TEM) imaging and diffraction was conducted on the sample after Pd deposition. Crystalline materials yield diffraction patterns with distinct spots, and amorphous materials yield diffraction patterns with concentric circles of varying brightness. The diffraction pattern for a sample after metal deposition is seen in Figure 3.2(b). Clear, distinct bright spots were observed, suggesting that the sample is still crystalline, and has not become amorphized during the shadow masking- metal deposition step.

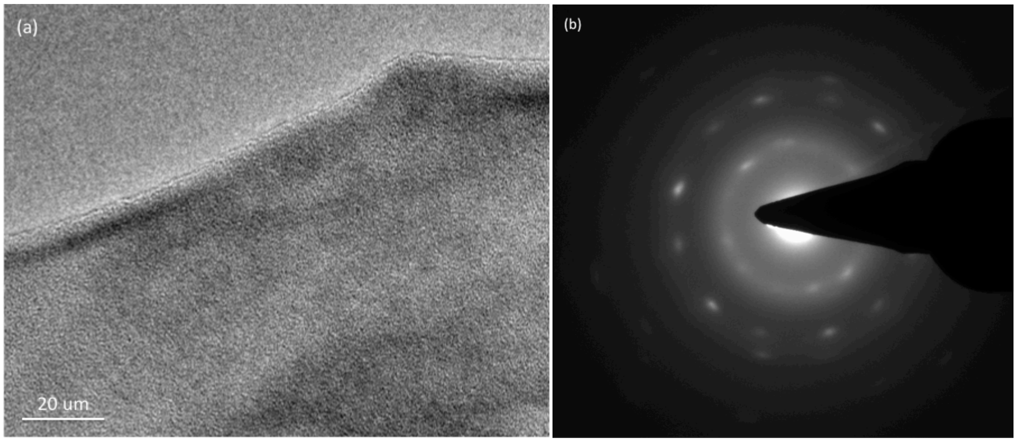

Figure 3.2: (a) TEM image of sample edge (b) sample diffraction pattern after shadow masking

Secondly, thermal conductivity experiments were conducted on another set of samples without metal deposition at the contacts. As previously mentioned, shadow masking-metal deposition at the contacts increases thermal contact between the sample and the device, and decreases thermal contact resistance. In order to compare experimental results of samples with and without metal deposition at the contacts, a contact resistance analysis was completed.

3.3 Contact Resistance and Experimental Results

The measured thermal resistance (R_m) sonsists of the diffusive resistance of the suspended sample (R_{sample}) and the thermal contact resistance (R_c), namely

$$R_m = R_{sample} + R_c \tag{3.1}$$

With R_{sample} expressed as a function of the length (L), thickness (t), and width (W) of the suspended segment, Equation 3.1 becomes

$$R_m = \frac{L}{\kappa t W} + R_c \tag{3.2}$$

With the use of interface resistance per unit width, R_c'

$$R_m = \frac{L}{\kappa t W} + \frac{R_c'}{W} \tag{3.3}$$

Or,

$$R_m W = \frac{1}{k}\frac{L}{t} + R_c{}' \tag{3.4}$$

where κ is the thermal conductivity of the sample, R_c' is determined by plotting the $R_{th}W$ vs. $\frac{L}{t}$ data for a given temperature. The *y*-intercept represents $R_c{}'$ and therefore contact resistance can be determined by dividing this value by the sample width. Figure 3.3 shows how this parameter was determined. All error bars are plotted, though some are too small to see.

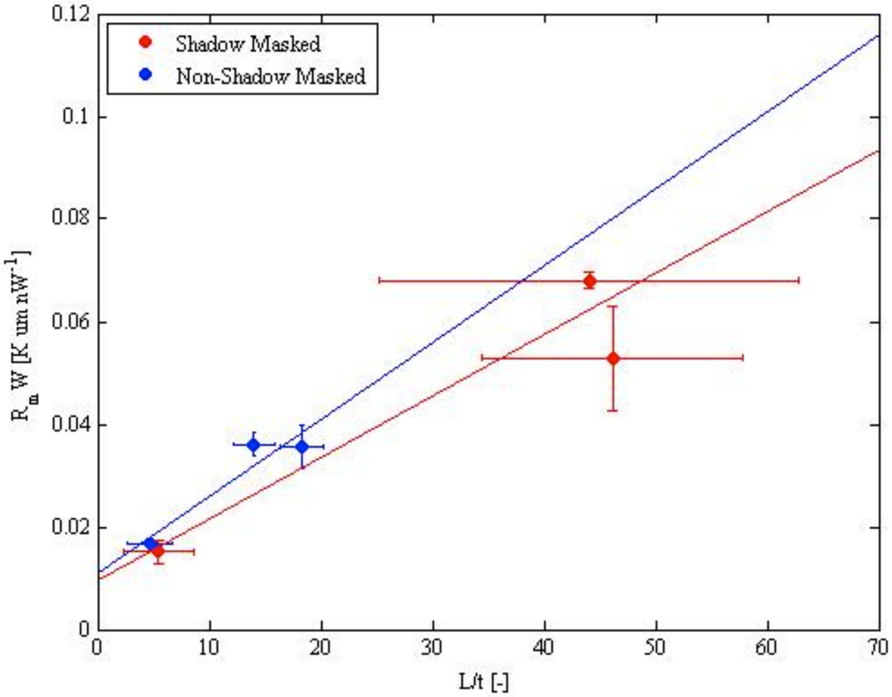

Figure 3.3: Determination of contact resistance for two sets of samples with and without metal deposition at the contacts

Finally, the thermal conductivity can be calculated by subtracting the calculated contact resistance from the measured thermal resistances, namely

$$R_s = R_m - R_c \tag{3.5}$$

$$\frac{L}{\kappa W t} = R_m - R_c \tag{3.6}$$

$$\kappa = \frac{L}{Wt(R_m - R_c)} \tag{3.7}$$

The experimentally determined values of thermal conductivity for both sets of samples are given in the figure below. Because the contact resistance makes a relatively large contribution to the two short samples, the uncertainty in the contact resistance results in relatively large uncertainty in the thermal conductivity determined for these two samples, compared to those for the four long samples, as shown in Fig. 3.4(1). For this reason, only the thermal conductivity determined for the four long samples have been included in Fig. 3.4(b). Samples 2,3, and 5 have undergone metal deposition, and Samples 14, 15, and 16 have not.

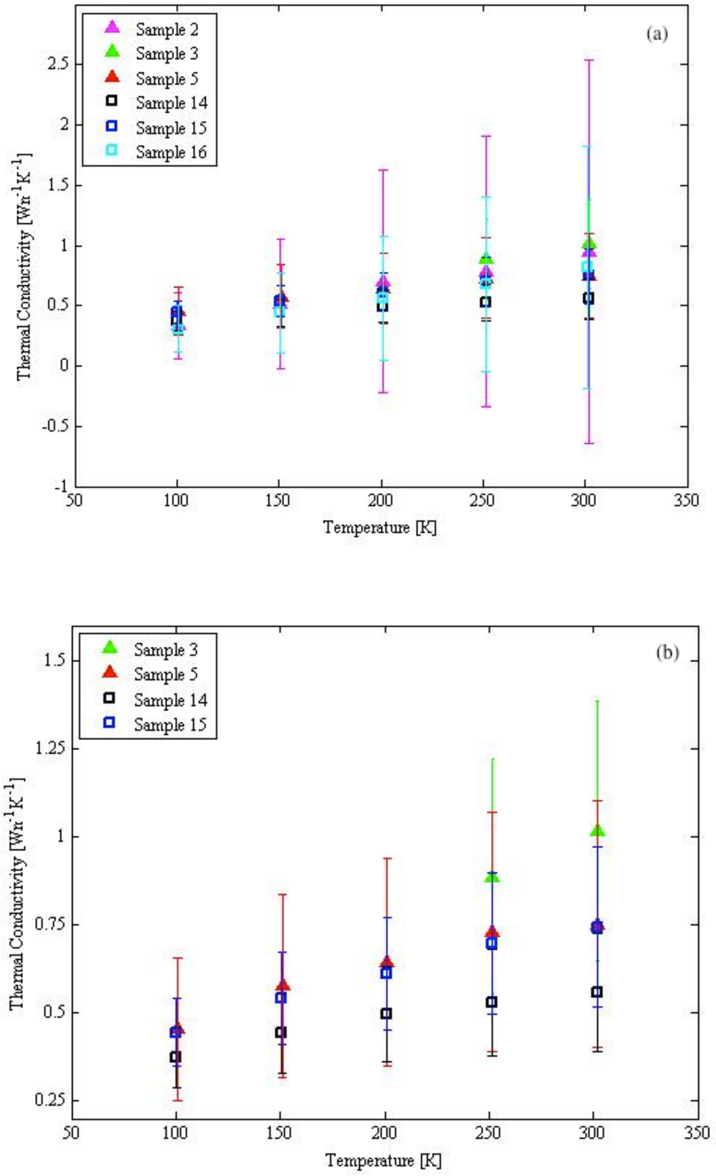

Figure 3.4: Experimentally determined in-plane thermal conductivity of suspended Germanane

After subtracting the contact resistances for each set of samples, it is observed that their thermal conductivities are similar. This finding is consistent with the TEM diffraction pattern of shadow-masked samples, and indicates that the samples were not amorphized by the metal deposition process.

3.4 Uncertainty Analysis

Uncertainty analysis was performed to determine the accuracy and precision of the data. The uncertainty sources come from the measured sample dimensions and sample conductances, which are propagated in the uncertainty in the contact resistance.

The sample dimensions were all measured using a scanning electron microscope (SEM). Multiple measurements were made across the suspended sample. The standard deviation of the measurements (σ_s) was used to obtain the uncertainty of the corresponding random uncertainty as

$$\delta X = t \frac{\sigma_X}{\sqrt{N}} \tag{3.8}$$

where t is the student t-distribution for 5% confidence and depends on the number of measurements. The obtained dimensions and uncertainties are shown in Table 3.1 for the six samples measured in this work.

Table 3.1: Sample dimensions and dimension uncertainties

Sample	***L* (μm)**	***δL* (μm)**	***W* (μm)**	***δW* (μm)**	***t* (μm)**	***δt* (μm)**
2	2.60	1.27	5.40	0.81	0.48	0.14
3	15.20	1.27	11.28	1.94	0.33	0.08
5	15.05	1.27	12.60	0.25	0.34	0.14
14	10.21	1.27	5.25	0.33	0.73	0.02
15	14.21	1.27	6.48	0.76	0.78	0.04
16	2.75	1.27	5.79	0.30	0.59	0.01

The uncertainties shown in Figure 3.3 were determined as follows:

$$\delta(R_{th}W) = \left[\left(\frac{\partial(R_{th}W)}{\partial R_{th}}\delta R_{th}\right)^2 + \left(\frac{\partial(R_{th}W)}{\partial W}\delta W\right)^2\right]^{1/2} \tag{3.9}$$

$$\delta(R_{th}W) = [(W\ \delta R_{th})^2 + (R_{th}\ \delta W)^2]^{1/2} \tag{3.10}$$

$$\delta\left(\frac{L}{t}\right) = \left[\left(\frac{\partial(L/t)}{\partial L}\delta L\right)^2 + \left(\frac{\partial(L/t)}{\partial t}\delta t\right)^2\right]^{1/2} \tag{3.11}$$

$$\delta\left(\frac{L}{t}\right) = \left[\left(-\frac{1}{t^2}\ \delta L\right)^2 + (L\ \delta t)^2\right]^{1/2} \tag{3.12}$$

As previously discussed, the contact resistances were determined by plotting the $R_{th}W$ vs. $\frac{L}{t}$ data for each of the two sample sets, and fitting a line to each set. Brown, Coleman, and Steel have created a method for determining experimental uncertainties in linear regression [24]. Here, let $X = \frac{L}{t}$ and $Y = R_{th}W$. The *y*-intercept, $c = R_{th}W\left(\frac{L}{t} = 0\right)$, is found by taking the following summations for each data set.

$$c = \frac{\sum_{i=1}^{N}(X_i)^2 \sum_{i=1}^{N} Y_i - \sum_{i=1}^{N} X_i \sum_{i=1}^{N}(X_i Y_i)}{N\sum_{i=1}^{N}(X_i)^2 - \left(\sum_{i=1}^{N} X_i\right)^2} \tag{3.13}$$

Assuming that the correlation between the *X* and *Y* errors is negligible in this measurement, the uncertainty in the *y*-intercept is given as:

$$\delta_c = \sqrt{\sum_{i=1}^{N}\left(\frac{\partial c}{\partial X_i}\right)^2 \delta_{X_i}^2 + \sum_{i=1}^{N}\left(\frac{\partial c}{\partial Y_i}\right)^2 \delta_{Y_i}^2} \tag{3.14}$$

Since the *y*-intercept is related to the contact resistance, now the uncertainty in contact resistance can be found as follows.

$$R_c = \frac{c}{W} \tag{3.15}$$

$$\delta R_c = \left[\left(\frac{\partial R_c}{\partial c}\delta c\right)^2 + \left(\frac{\partial R_c}{\partial W}\delta W\right)^2\right]^{1/2} \tag{3.16}$$

$$\delta R_c = \left[\left(\frac{\delta c}{W}\right)^2 + \left(\frac{-c}{W^2}\delta W\right)^2\right]^{1/2} \tag{3.17}$$

The uncertainty in the measured sample conductance is determined by examining the random and bias uncertainties from the measurement. The random uncertainty, $\delta G_{m,R}$ were calculated using Eq. 3.8. The bias uncertainty, $\delta G_{m,B}$, is determined from the calibration of the experimental instrumentation. The total uncertainty of the sample conductance is given as:

$$\delta G_m = G_m\sqrt{\delta G_{m,R}^2 + \delta G_{m,B}^2} \tag{3.18}$$

Since sample resistance and conductance have a reciprocal relationship, the uncertainty in the sample resistance can be calculated.

$$R_{th} = \frac{1}{G_m} \tag{3.19}$$

$$\delta R_{th} = \frac{\partial R_{th}}{\partial G_m}\,\delta G_m \tag{3.20}$$

$$\delta R_{th} = \frac{-1}{G_m^2}\,\delta G_m \tag{3.21}$$

Finally, having calculated the uncertainties of each component, the uncertainty in thermal conductivity can be calculated from Eq. 3.7.

$$\delta\kappa = \left[\left(\frac{\partial\kappa}{\partial L}\delta L\right)^2 + \left(\frac{\partial\kappa}{\partial W}\delta W\right)^2 + \left(\frac{\partial\kappa}{\partial t}\delta t\right)^2 + \left(\frac{\partial\kappa}{\partial R_m}\delta R_m\right)^2 + \left(\frac{\partial\kappa}{\partial R_c}\delta R_c\right)^2\right]^{1/2} \quad (3.22)$$

$$\frac{\partial\kappa}{\partial L} = \frac{1}{Wt}\cdot\frac{1}{R_m - R_c} \quad (3.23)$$

$$\frac{\partial\kappa}{\partial W} = \frac{-L}{W^2 t}\cdot\frac{1}{R_m - R_c} \quad (3.24)$$

$$\frac{\partial\kappa}{\partial t} = \frac{-L}{W t^2}\cdot\frac{1}{R_m - R_c} \quad (3.25)$$

$$\frac{\partial\kappa}{\partial R_m} = \frac{L}{Wt}\cdot - \frac{1}{(R_m - R_c)^2} \quad (3.26)$$

$$\frac{\partial\kappa}{\partial R_c} = \frac{L}{Wt}\cdot\frac{1}{(R_m - R_c)^2} \quad (3.27)$$

3.5 Discussion

A phonon is a quantized description of vibrations within atoms in a lattice. Thermal conductivity in non-metals, like Germanane, is mostly caused by phonons. A phonon's mean free path is defined as the average distance it travels before scattering and losing its energy. The further a phonon can travel without scattering, i.e. the longer its mean free path, the better the material will conduct heat. For isotropic crystals, the simple kinetic theory gives the thermal conductivity as

$$\kappa = \frac{1}{3}Cv\Lambda \quad (3.28)$$

where κ is the thermal conductivity, C is the volumetric specific heat, v is the phonon group velocity, and Λ is the phonon mean free path.

Graphene, a single-atom thick carbon sheet, is a material with one of the highest-reported thermal conductivities [5, 25]. This is due to its sp^2-bonded structure, which allows for long phonon mean free paths because the phonons are able to travel freely through the graphene without scattering. Theoretical studies have been conducted on hydrogenated graphene, graphane, and show that the hydrogenation of graphene reduces the thermal conductivity of graphene by 80% [26]. This is due to the change in the material structure from sp^2- to sp^3- bonding as the graphene becomes hydrogenated. The sp^3 bonds scatter the phonons, reducing their mean free path, and lowering the material's thermal conductivity.

Studies have also been conducted on the affects of single- versus multi-layer graphene. As the number of layers increases, so does the phonon-phonon scattering between layers, leading to a decrease in thermal conductivity. At room temperature, the thermal conductivity of graphene only five layers thick already approaches that of build graphite, and is ~65% of single-layer graphene [27].

Bulk crystalline Germanium (Ge) has a thermal conductivity of 58 $Wm^{-1}K^{-1}$, and thin-film Ge is predicted to approach 30 $Wm^{-1}K^{-1}$ with increasing film thickness [28]. Here, 330-780nm-thick, multi-layer GeH was measured. Similar to the hydrogenated graphene, GeH has an sp^3- bonded structure. Defects in the hydrogen termination can result in phonon scattering, reducing the phonon mean free path and lowering the material thermal conductivity. Scattering can also be caused by interactions between GeH layers. These factors must have been responsible for the observed much lower thermal conductivity in the GeH samples, compared to that in Ge thin film and bulk materials.

Chapter 4

Conclusion

This work is focused on the characterization of in-plane thermal transport in Germanane, thin stacks of hydrogen-terminated layered germanium. Two sets of samples were measured: one with, and the other without, metal deposition at the contacts. Transmission electron microscopy (TEM) measurement results suggest that metal deposition at the contacts did not cause amorphization of the sample. For each sample, the thermal contact resistance was obtained from the measured thermal resistance values of three samples of different suspended lengths. The values of in-plane thermal conductivity determined for both samples are similar, between 0.56-1.01 $Wm^{-1}K^{-1}$ at room temperature. The low values of thermal conductivity are attributed to phonon scattering by defects both within the layers and at the layer-layer interfaces in the GeH samples.

Although the low thermal conductivity is desirable for increasing the thermoelectric figure of merit, the Seebeck coefficient and electrical conductivity of the samples have not been measured in the undoped samples. It is recommended that future works continue to characterize these thermoelectric properties of doped Germanane. Once these parameters are determined, its potential as a new material for next-generation thermoelectric devices can be better determined.

Bibliography

[1] Estimated U.S. Energy Use in 2013. [Online]. https://flowcharts.llnl.gov/content/energy/energy_archive/energy_flow_2013/2013USEnergy.png (accessed April 28, 2014)

[2] L.-D. Zhao, S.-H. Lo, Y. Zhang, H. Sun, G. Tan, C. Uher, C. Wolverton, V. P. Dravid, and M. G. Kanatzidis, "Ultralow thermal conductivity and high thermoelectric figure of merit in SnSe crystals," *Nature*, vol. 508, no. 7496, pp. 373–377, Apr. 2014.

[3] E. Muñoz, A. K. Singh, M. a. Ribas, E. S. Penev, and B. I. Yakobson, "The ultimate diamond slab: GraphAne versus graphEne," *Diam. Relat. Mater.*, vol. 19, no. 5–6, pp. 368–373, May 2010.

[4] S. Z. Butler, S. M. Hollen, L. Cao, Y. Cui, J. A. Gupta, H. R. Gutie, T. F. Heinz, S. S. Hong, J. Huang, A. F. Ismach, E. Johnston-halperin, M. Kuno, V. V Plashnitsa, R. D. Robinson, R. S. Ruoff, S. Salahuddin, J. Shan, L. Shi, O. M. G. Spencer, M. Terrones, W. Windl, and J. E. Goldberger, "Opportunities in Two-Dimensional Materials Beyond Graphene," no. 4, pp. 2898–2926, 2013.

[5] A. A. Balandin, "Thermal properties of graphene and nanostructured carbon materials.," *Nat. Mater.*, vol. 10, no. 8, pp. 569–81, Aug. 2011.

[6] J. C. Garcia, D. B. de Lima, L. V. C. Assali, and J. F. Justo, "Group IV Graphene- and Graphane-Like Nanosheets," *J. Phys. Chem. C*, vol. 115, no. 27, pp. 13242–13246, Jul. 2011.

[7] R. Cheaito, J. C. Duda, T. E. Beechem, K. Hattar, J. F. Ihlefeld, D. L. Medlin, M. a. Rodriguez, M. J. Campion, E. S. Piekos, and P. E. Hopkins, "Experimental Investigation of Size Effects on the Thermal Conductivity of Silicon-Germanium Alloy Thin Films," *Phys. Rev. Lett.*, vol. 109, no. 19, p. 195901, Nov. 2012.

[8] X. Zhang, H. Xie, M. Hu, H. Bao, S. Yue, G. Qin, and G. Su, "Thermal conductivity of silicene calculated using an optimized Stillinger-Weber potential," *Phys. Rev. B*, vol. 89, no. 5, p. 054310, Feb. 2014.

[9] E. Bianco, S. Butler, S. Jiang, O. D. Restrepo, W. Windl, and J. E. Goldberger, "Stability and Exfoliation of Germanane : A Germanium Graphane Analogue," no. 5, pp. 4414–4421, 2013.

[10] J. Lee, D. Yoon, H. Kim, S. W. Lee, and H. Cheong, “Thermal conductivity of pristine suspended graphene using Raman spectroscopy,” no. c, pp. 1–4, 2011.

[11] Z. Yan, C. Jiang, T. R. Pope, C. F. Tsang, J. L. Stickney, P. Goli, J. Renteria, T. T. Salguero, and a. a. Balandin, “Phonon and thermal properties of exfoliated TaSe2 thin films,” *J. Appl. Phys.*, vol. 114, no. 20, p. 204301, 2013.

[12] T. Raman, R. Yan, J. R. Simpson, S. Bertolazzi, J. Brivio, M. Watson, X. Wu, A. Kis, T. Luo, A. R. H. Walker, and H. G. Xing, “Thermal Conductivity of Monolayer Molybdenum Disulfide Obtained from Temperature-Dependent Raman Spectroscopy,” pp. 986–993, 2014.

[13] C. A. Paddock and G. L. Eesley, “Transient thermoreflectance from thin metal films,” *J. Appl. Phys.*, vol. 60, no. 1, p. 285, 1986.

[14] B. M. Foley, H. J. Brown-Shaklee, J. C. Duda, R. Cheaito, B. J. Gibbons, D. Medlin, J. F. Ihlefeld, and P. E. Hopkins, “Thermal conductivity of nano-grained SrTiO[sub 3] thin films,” *Appl. Phys. Lett.*, vol. 101, no. 23, p. 231908, 2012.

[15] M. S. Aubain and P. R. Bandaru, “Determination of diminished thermal conductivity in silicon thin films using scanning thermoreflectance thermometry,” *Appl. Phys. Lett.*, vol. 97, no. 25, p. 253102, 2010.

[16] S. D. Kang, J. Joon Yoo, H.-K. Lyeo, J. Yong Song, S. Lee, and J. Yu, “Assessing the thermal conductivity of non-uniform thin-films: Nanocrystalline Cu composites incorporating carbon nanotubes,” *J. Appl. Phys.*, vol. 110, no. 2, p. 023506, 2011.

[17] G. A. Antonelli, B. Perrin, B. C. Daly, and D. G. Cahill, “Characterization of Mechanical and Thermal Properties Using Ultrafast Optical Metrology,” vol. 31, no. August, pp. 607–613, 2006.

[18] D. G. Cahill, “Thermal conductivity measurement from 30 to 750 K: the 3ω method,” *Rev. Sci. Instrum.*, vol. 61, no. 2, p. 802, 1990.

[19] J. Jin, M. P. Manoharan, Q. Wang, and M. a. Haque, “In-plane thermal conductivity of nanoscale polyaniline thin films,” *Appl. Phys. Lett.*, vol. 95, no. 3, p. 033113, 2009.

[20] T. S. Pan, Y. Zhang, J. Huang, B. Zeng, D. H. Hong, S. L. Wang, H. Z. Zeng, M. Gao, W. Huang, and Y. Lin, “Enhanced thermal conductivity of polycrystalline aluminum nitride thin films by optimizing the interface structure,” *J. Appl. Phys.*, vol. 112, no. 4, p. 044905, 2012.

[21] H. Wang and M. Sen, “Analysis of the 3-omega method for thermal conductivity measurement,” *Int. J. Heat Mass Transf.*, vol. 52, no. 7–8, pp. 2102–2109, Mar. 2009.

[22] T. Tong and A. Majumdar, “Reexamining the 3-omega technique for thin film thermal characterization,” *Rev. Sci. Instrum.*, vol. 77, no. 10, p. 104902, 2006.

[23] L. Shi, D. Li, C. Yu, W. Jang, D. Kim, Z. Yao, P. Kim, and A. Majumdar, “Measuring Thermal and Thermoelectric Properties of One-Dimensional Nanostructures Using a Microfabricated Device,” *J. Heat Transfer*, vol. 125, no. 5, p. 881, 2003.

[24] K. K. Brown, H. W. Coleman, and W. G. Steele, “A Methodology for Determin Experimental Uncertainties iin ng Regressions,” vol. 120, no. September 1998, 2014.

[25] M. M. Sadeghi, M. T. Pettes, and L. Shi, “Thermal transport in graphene,” *Solid State Commun.*, vol. 152, no. 15, pp. 1321–1330, Aug. 2012.

[26] Q.-X. Pei, Z.-D. Sha, and Y.-W. Zhang, “A theoretical analysis of the thermal conductivity of hydrogenated graphene,” *Carbon N. Y.*, vol. 49, no. 14, pp. 4752–4759, Nov. 2011.

[27] Z. Wei, Z. Ni, K. Bi, M. Chen, and Y. Chen, “In-plane lattice thermal conductivities of multilayer graphene films,” *Carbon N. Y.*, vol. 49, no. 8, pp. 2653–2658, Jul. 2011.

[28] Z. H. Wang and M. J. Ni, “Thermal conductivity and its anisotropy research of germanium thin film,” *Heat Mass Transf.*, vol. 47, no. 4, pp. 449–455, Dec. 2010.